Eur. J. Mech. B - Fluids 20 (2001) 673–698

S0997-7546(01)01144-X/FLA

Near field vortex dynamics in axially forced, laminar, co-flowing jets: a descriptive study of the flow configurations

Pedro Rodríguez-Aumente, Ulpiano Ruiz-Rivas *, Antonio Lecuona

Departamento de Ingeniería Mecánica, Escuela Politécnica Superior, Universidad Carlos III de Madrid, Spain

(Received 5 June 2000; revised 19 February 2001; accepted 11 April 2001)

Abstract – An experimental study is presented of the vortex structures that appear in the shear layer of laminar, co-flowing air jets subjected to strong axial forcing. A set of flow visualisation experiments has been performed to elucidate the nature of the different structures and the mechanisms leading to their appearance and further interactions. The axial forcing sets the axisymmetric instability to prescribed values of amplitude and frequency (and thus wavelength) and produces a strong effect in the lateral spreading of the inner jet. It is shown that the near field development of the flow can be explained via inviscid vortex dynamics arguments, involving three vortex structures. Due to the strong axial forcing, all these vortices already appear as developed concentrations of vorticity in the surroundings of the nozzle exit. An azimuthal perturbation is added to the flow in the form of a lobed nozzle exit, in order to lock the azimuthal organisation of the vortices. The results are discussed and some representative configurations are examined. Each configuration appears for a given range of the forcing parameters. A tentative model of the near-field vortex dynamics is developed, but quantitative measurements are still necessary. © 2001 Éditions scientifiques et médicales Elsevier SAS

vortex dynamics / forced flow / co-flowing jets / air jet

1. Introduction

The axisymmetric instability of a laminar, cylindrical shear layer has been extensively studied [1–5]. It results in the roll up of the vorticity sheet to form a periodic array of vortex rings. Yule [6], Tso and Hussain [7] and several other authors have observed a similar behaviour in the development of transitional and turbulent jets.

Furthermore, a secondary instability appears as the vortex rings develop an azimuthal organisation, leading to the transition to three-dimensionality. This instability has been studied either as a vortex ring instability or as a braid instability. As an instability of the ring-like vortices, it has been associated with the short-wave instability found in isolated vortex rings, usually known as the Widnall instability. This problem has been studied in detail, both analytically and experimentally [8,9]. Corcos and co-workers [10,11] have studied the braid instability for a plane shear layer. In shear layers, the strain field generated by the strong vortices (resulting from the primary instability) re-directs in the streamwise direction and amplifies a residual vortex structure that appears in the braids. Due to this effect, the secondary structure is often referred to as a 'streamwise structure'. The origin and development of this structure and its interaction with the one caused by the primary instability has been intensively studied, theoretically, numerically, and experimentally, for plane shear layers [10–21]. There are also several works related to 2D wakes [22–25] and axisymmetric jets [26–30], among others. The works of Williamson [31] suggest that a general agreement has been reached for cylinder wakes, but the three-dimensional transition mechanisms for axisymmetric jets are not completely understood.

* Correspondence and reprints.
E-mail address: ulpiano@ing.uc3m.es (U. Ruiz-Rivas).

The present study is restricted to low Mach number, laminar flows. A set of flow visualisation experiments was conducted on co-flowing jets, in which the inner jet was subjected to strong axial forcing and an azimuthal perturbation was added at the nozzle exit. The aim of this paper is not to draw conclusions on the natural flow through the study of the characteristics of the perturbed flow. The flow is strongly forced to saturate and consequently fix the frequency/wavelength of the instabilities, developing in the near field structures of concentrated vorticity. Thus, comparison of the dynamics observed with those of a natural flow, even in its far field, is not straightforward.

Therefore, the aim of this paper is to study the effect of an axial monochromatic forcing of finite amplitude in the development of co-flowing jets. The varying parameters will be the amplitude and the frequency of the monochromatic forcing.

In a previous article [32], the three-dimensional structure of the vorticity field was studied using the same experimental facility. The results showed that, depending on the frequencies and amplitudes of the perturbations, four typical 'modes' or arrangements of the vorticity appear. These 'modes' were clearly defined, but no attempt was made to characterise the mechanisms that lead to their appearance, although some interesting suggestions were made. The article showed that the use of finite amplitude, single frequency axial forcing, combined with single frequency azimuthal perturbation, could largely enhance the lateral spread of the jet. This can be of interest to the development of better mixers, ejectors, and nozzles for industrial devices. In this sense, the work of Monkiewitz and Pfizenmaier [33] in self-excited (heated or with density gradients) and strongly forced jets is of particular interest, as it suggests a strong relation of the mechanisms controlling both flows.

Two different sets of experiments were performed for this study. The first set is intended to explore the different configurations of the flow, depending on the forcing parameters (frequency and amplitude). The second set focuses in one simple configuration and its aim is to study the 3D dynamics of the structures that appear in the near field. Extensive visualisations with transverse and longitudinal phase-lock cuts of the shear layer were performed to obtain a 3D reconstruction of the evolving flow. The second set configuration was chosen for its relative simplicity. This is determined by a low forcing frequency, which gives a large wavelength of the vortex rings and therefore, more distinct structures. Nevertheless, the configuration is sufficiently complex to give a comprehensive view of the mechanisms that drive the different configurations.

The visualisation of vortical structures has its well-known drawbacks, as shown by Hussain [34] and other authors. Nevertheless, it has been generally assumed in the past [12,15,16,18,25], etc. that, in the near field of a free shear layer, vorticity is present where the mixing layer shows a rollup. In zones of high stretching, this link between a passive concentration field and the vorticity field can induce errors, mostly if just one measurement (image) is taken. To diminish as much as possible this risk of misinterpretation of the vorticity field structure, phase lock measurements have been obtained. They show a time sequence of the flow development, which permits to observe the evolution of the passive rolls. In most cases, the phase-locked measurements reveal that these rolls are constantly growing. This evidence reinforce the assumption of the existence of vorticity where a roll up appears.

As a continuation of this work, the authors are studying a hydrodynamic flow subjected to a similar forcing. The Reynolds number is an order of magnitude higher, but the configurations seem to be quite similar. This was expected, due to the inviscid nature of the processes. In those experiments, the vorticity field was obtained from 2D-PIV velocity maps. Preliminary results are given in Ruiz-Rivas et al. [35].

2. Experimental facility

The experiments were conducted in an atmospheric pressure, open return wind tunnel. *Figure 1* shows a layout of the flow facility. Only a short description of the facility will be given here. Lasheras et al. [32] offers a more detailed explanation.

The wind tunnel consists of three independently created, low speed, axisymmetric streams. The inner stream is produced through a nozzle of diameter $D = 25.4$ mm, connected through a long tube with a settling chamber, where a combination of gases can be independently metered. A slower, co-flowing, coaxial gas stream surrounds the inner jet. It discharges on the test section through a round nozzle of 160 mm of diameter. Atmospheric air is drawn into the test section forming an additional low speed, external, co-flowing jet. This third stream is intended for combustion experiments; in our cold experiments, it just serves to avoid re-circulation due to jet entrainment. The three co-flowing jets meet in a box of 440×440 mm square cross section, which is 1200 mm high and has lateral walls of transparent metacrilate. LDV velocity measurements showed that, for any selected flow conditions, the turbulence intensities of the exit profile of the natural flow were always less than 1%.

The axial forcing is produced through a vibrating membrane, located at the bottom end of the settling chamber of the inner flow, and it is driven by a loudspeaker fed with a sinusoidal wave. The membrane fluctuation adds a monochromatic axial velocity excitation of a given amplitude and frequency, f, to the inner jet flow.

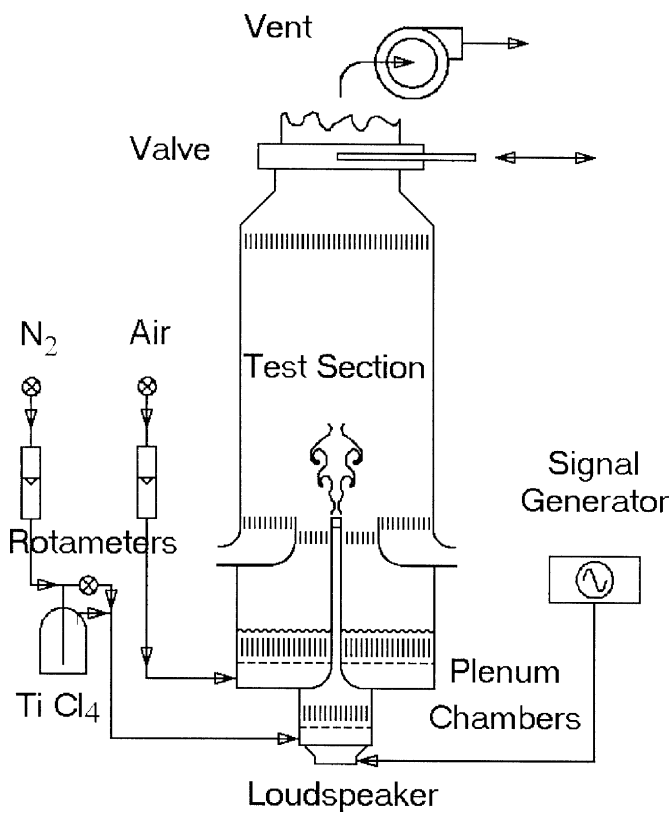

Figure 1. Layout of the flow facility.

The relevant dimensionless parameters of the flow are:

$$Re = \frac{(u_{i,\text{mean}} - u_o)D}{\nu}, \qquad St = \frac{fD}{(u_{i,\text{mean}} + u_o)/2},$$
$$A_z = \frac{u_{i,\max} - u_{i,\min}}{2u_{i,\text{mean}}} = \frac{u_{i,\max} - u_{i,\min}}{u_{i,\max} + u_{i,\min}}, \qquad u_R = \frac{u_{i,\text{mean}} - u_o}{u_{i,\text{mean}} + u_o}, \tag{1}$$

where $u_{i,\text{mean}}$, $u_{i,\max}$, and $u_{i,\min}$ are, respectively, the mean, maximum and minimum inner jet velocities (measured on the axis) in a forcing cycle, ν is the air kinematic viscosity and u_o is the (mean) outer jet velocity. The definition of the Strouhal number, *St*, is intended to represent a ratio between the integral length scale of the flow (D) and the wavelength of the primary instability.

The results reported here correspond to an inner flow mean velocity of 0.48 m/s (measured on the axis) and an outer flow mean velocity of 0.22 m/s. The axial forcing frequencies ranged from 10 to 40 Hz. For those conditions, the dimensionless parameters have the following values:

$$Re = 420, \qquad St = 0.7 \to 3, \qquad A_z = 0 \to 100\%, \qquad u_R = 0.37.$$

The inner and outer flow velocities have been chosen in order to have a laminar flow (low Reynolds number) and a relatively high velocity ratio (low u_R). The reason for addressing the laminar flow is that it is simpler, this being a first study of this complex flow configuration. As stated before, some preliminary studies (Ruiz-Rivas et al. [35], Prestidge [36,37]) have shown that the flow structures are similar for higher Reynolds numbers. The high velocity ratio is intended to enhance the outer influence on the flow evolution, thoroughly changing from the well-known configuration of a jet discharging into a quiescent atmosphere.

An azimuthal perturbation was introduced by using corrugated or indented nozzles. The profiles of the lobes (sinusoidal or rectangular) and the direction of perturbation (profiles developing in the axial direction – indented – or in the radial direction – corrugated) were systematically changed and their influence was assessed. In both cases, the sinusoidal profile had ±2.5 mm amplitude and the number of waves per revolution was set to five. This is near to the most unstable number of waves that are amplified through the instability of the ring. This number, as calculated by Brancher et al. [30], based on the model of Pierrehumbert and Widnall [38], depends on the instantaneous maximum velocity of the flow (and thus on the forcing amplitude, which is a changing parameter in these experiments). The number we have chosen is of the same order as that calculated from the model of [38], and coincides with the experimental data referenced by Martin and Meiburg [28]. *Figure 2* shows sketches of nozzles having sinusoidal indentations and corrugations and defines the nomenclature adopted for comparison.

3. Flow visualisation technique

A combination of flow visualisation techniques was used in this study. The inner flow, consisting of N_2 with a negligible concentration of water vapour, is saturated with $TiCl_4$ vapour and subsequently injected in the settling chamber. *Figure 1* shows a schematic of the configuration. The co-flowing airflow consists of atmospheric humid air. As the two streams meet at the edge of the nozzle, the $TiCl_4$ vapour reacts with the water vapour to form sub-micron sized TiO_2 particles. This reaction continues to occur as the jet develops. The reaction provides a continuous generation of scattering particles of low diffusivity (TiO_2) that will mark the instantaneous position of the mixing layer. The visualisation of such an interface is then achieved by recording the light scattered by the TiO_2 particles from longitudinal and crosscut laser light sheets, created by means of cylindrical lenses. *Figure 3* shows a schematic of the technique employed.

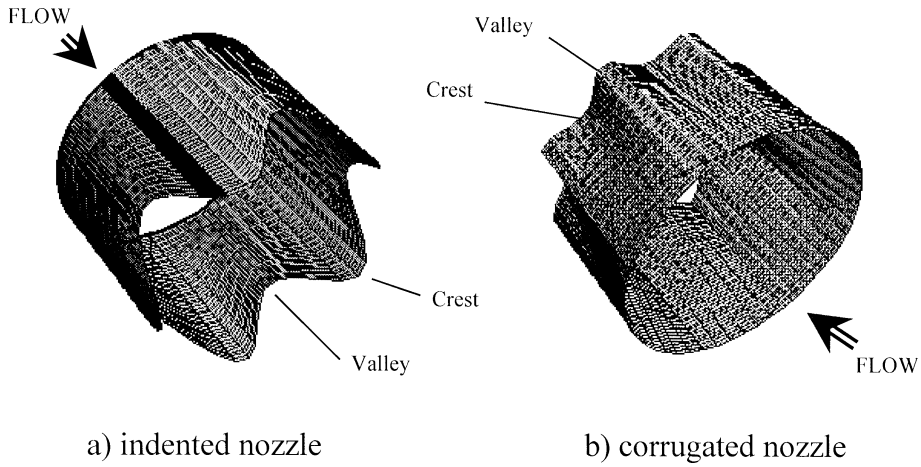

Figure 2. Outlet of five-lobes indented and corrugated nozzles: (a) left: indented nozzle; (b) right: corrugated nozzle.

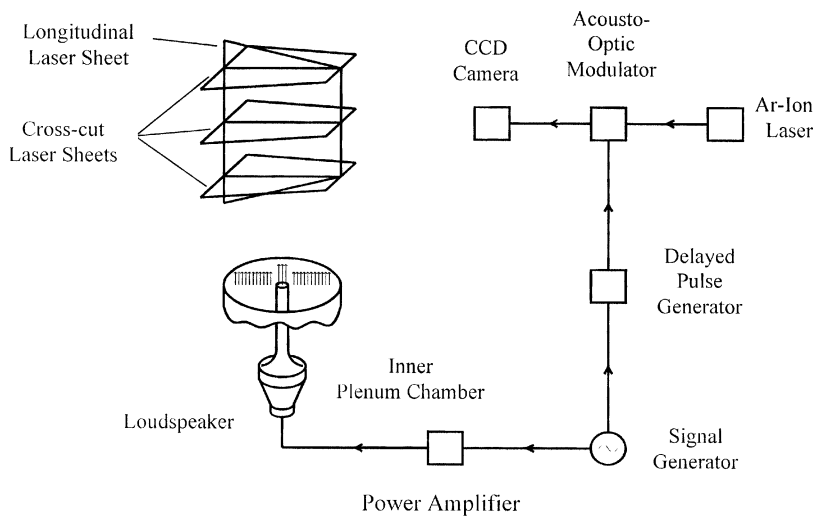

Figure 3. Scheme of the visualisation techniques arrangement.

4. Results

As it has been stated before [32], the structure of the near field is observed to change considerably when applying a strong axial forcing (see *figure 4*). The vorticity concentrates at the surroundings of the nozzle exit, forming different eddies, whose interface is observed in the images. The images shown are longitudinal cuts of the flow along its axis and, therefore, the eddies correspond to concentrations of azimuthal vorticity. The first image shows the mixing layer development in the unforced case. The shear layer is not observed to develop an instability in the observed region, but this natural instability will take place further downstream, thus forming the typical array of vortex rings. The two other images show forced cases with the same forcing frequency and different forcing amplitudes. In these cases, the geometry of the mixing layer becomes extremely complex, as the flow develops downstream of the nozzle exit. However, in the vicinity of the nozzle exit one can observe two eddies. They suggest the existence (in an incipient grade of development) of two vortices. The eddy placed nearest to the nozzle exit (a1, a2) is characteristic in jet development. It is induced by a concentrated vortex

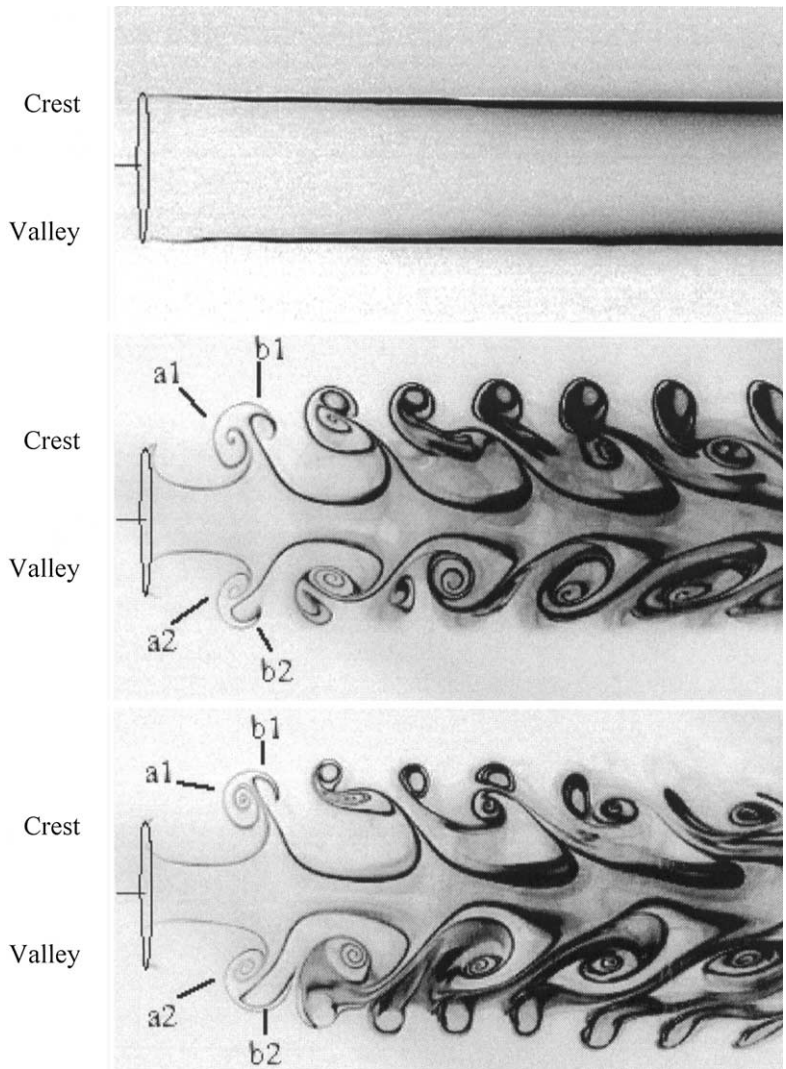

Figure 4. Different flow configurations. Flow comes from left to right. The 5-lobes corrugated nozzle exit is indicated in the left side, with a crest on top and a valley on bottom. The images are the negatives of the actual pictures, so the zones of formation of the TiO_2 particles can be seen in black. The axial forcing increases from the top image (unforced case) to the bottom image.

ring. This ring is similar to those that will appear in a natural jet, but it appears nearer to the nozzle exit due to the strong forcing. One can say that, as the axial forcing increases (in a low forcing frequency case), this vortex rings will become more and more similar to isolated vortex rings (for example, those due to a piston impulse or those observed in an impulsive-like start). The second eddy (b1, b2) is located in the downstream side of the first one and has the opposite sign of rotation. This eddy does not appear in a natural jet or for low forcing conditions, and seems to be of paramount importance to the flow development, as one can see in *figure 4*. The existence of a counter-rotating vortex ring is not characteristic of jet flows, nevertheless, the eddy seems to grow as it develops downstream, suggesting the existence of such vorticity field. The origin of this vortex should be intimately linked with the forcing applied, and it will be studied in the next section.

The azimuthal organisation of the rings cannot be observed in *figure 4*, but it can be stated that there are small differences between the eddies on the upper side (a1–b1 and followings) and those on the lower side (a2–b2

and followings). These differences represent the effect of the azimuthal perturbation imposed at the nozzle exit. It can be seen that, although its effect is small over the first two eddies, the perturbation is amplified as the jet develops and the differences between upper and lower organisation of the mixing layer increase. Moreover, the different development of the flow in the two forced images of *figure 4* is due to a change in the axial forcing amplitude (that will be quantified in the following section). These images synthesise the purpose of this study in understanding:

(i) the appearance of the counter-rotating ring in the surroundings of the nozzle exit;
(ii) the dynamics involved in the development of the flow (causing a strong azimuthal asymmetry and producing the lateral advance of the inner jet fluid);
(iii) the influence of the axial forcing range on the flow development.

4.1. Different flow configurations depending on the forcing parameters

In the last section it has been stated that the axial forcing amplitude has a strong effect on the jet development. *Figure 5* shows different flow configurations for conditions defined by: $Re = 420$, $u_R = 0.37$, $St = 0.94$. The forcing amplitude increases from top to bottom and its approximate value can be seen at the right side of each image.

Image 1 shows a low (relatively speaking) forcing amplitude case ($A_z \approx 25\%$). The forcing saturates the primary instability of the jet, providing a structure of equi-spaced vortex rings. The other structure, of counter-rotating vortex rings, eventually forms, but it is not clear. Here, the counter-rotating ring, if it exists, must have a very small circulation. Nevertheless, the image show traces of this counter-rotating structure on azimuthal positions aligned with a "crest" of the corrugated nozzle.

Image 2 shows the 35% forcing case. Here, the counter-rotating rings are better defined in the early stages, causing a stronger lateral spread as the flow develops downstream. But image 3 shows a change in this tendency of larger lateral spreads for increasing forcing amplitudes. Here, the lateral spread is truncated at an intermediate stage, although the forcing amplitude has been increased and the counter-rotating ring may seem evident. Image 4 shows that, for higher forcing amplitudes ($A_z \approx 45\%$), the crest lateral spread continues to diminish and, in turn, a lateral spread begins to show on the azimuthal positions aligned with a 'valley' of the corrugated nozzle. Note that the two initial vortex rings (that form a mushroom-like structure) show very similar between images 2, 3 and 4, and only a small change of the forcing amplitude causes the change in the observed geometry.

Finally, image 5 shows a very high forcing amplitude case ($A_z \approx 70\%$). The lateral spread in the valley-aligned positions is now larger and the evidence of the two counter-rotating rings is not clear after the first mushroom-like structure.

Similar configurations appear when changing the Strouhal number, but the forcing amplitude ranges for the different cases may vary. *Figure 6* shows the different passive scalar fields for increasing forcing frequencies. One can see that the configuration of two counter-rotating vortex rings appears in all cases at the surroundings of the nozzle exit, but the flow development varies in each case. The tendency explained before (of low forcing occurrence of lateral spread in positions aligned with crest, and then a change to lateral spread in positions aligned with the valleys) is confirmed.

Martin and Meiburg [28] and several other authors presented the possibility of the lateral ejection of inner fluid in the form of laterally developing closed vortex loops. This process involves a reconnection of highly stretched vortices and it may take place for the high amplitude images of *figures 5* and *6*. Nevertheless, the information given in this paper cannot be conclusive, because the passive scalar field visualized in these experiments can differ considerably from the vorticity field in a stretched zone.

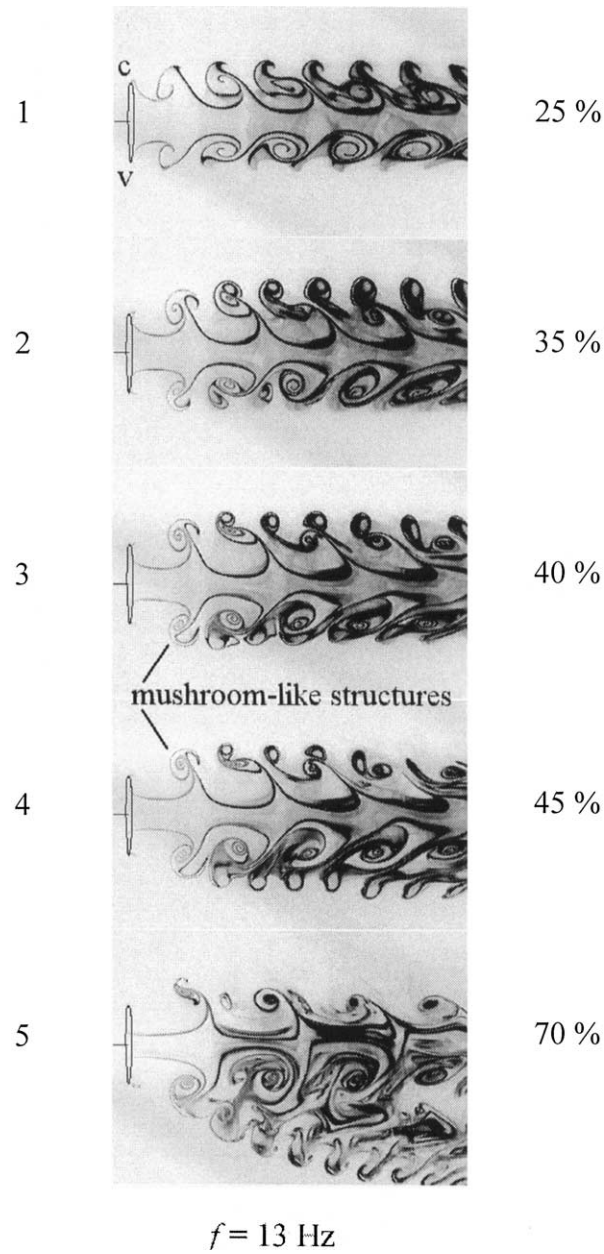

Figure 5. Longitudinal cuts along the flow axis for varying forcing amplitude. The flow conditions, as defined from equations (1), are $Re = 420$, $u_R = 0.37$ and $St = 0.94$. Flow comes from left to right. A crest (c) of the corrugated nozzle is on top and a valley (v) on bottom. The respective forcing amplitudes can be seen on the right side.

The experimental evidence already shown indicates the appearance of different lateral spreading configurations of the flow, depending on the forcing conditions. A complete study has been performed in order to obtain a map of the threshold values of the forcing parameters, over which the lateral spread of the flow changes considerably. *Figure 7* shows this map. The x-axis shows the Strouhal number. Two curves are drawn, giving the threshold values of the forcing amplitude for the appearance of a lateral spread configuration in positions

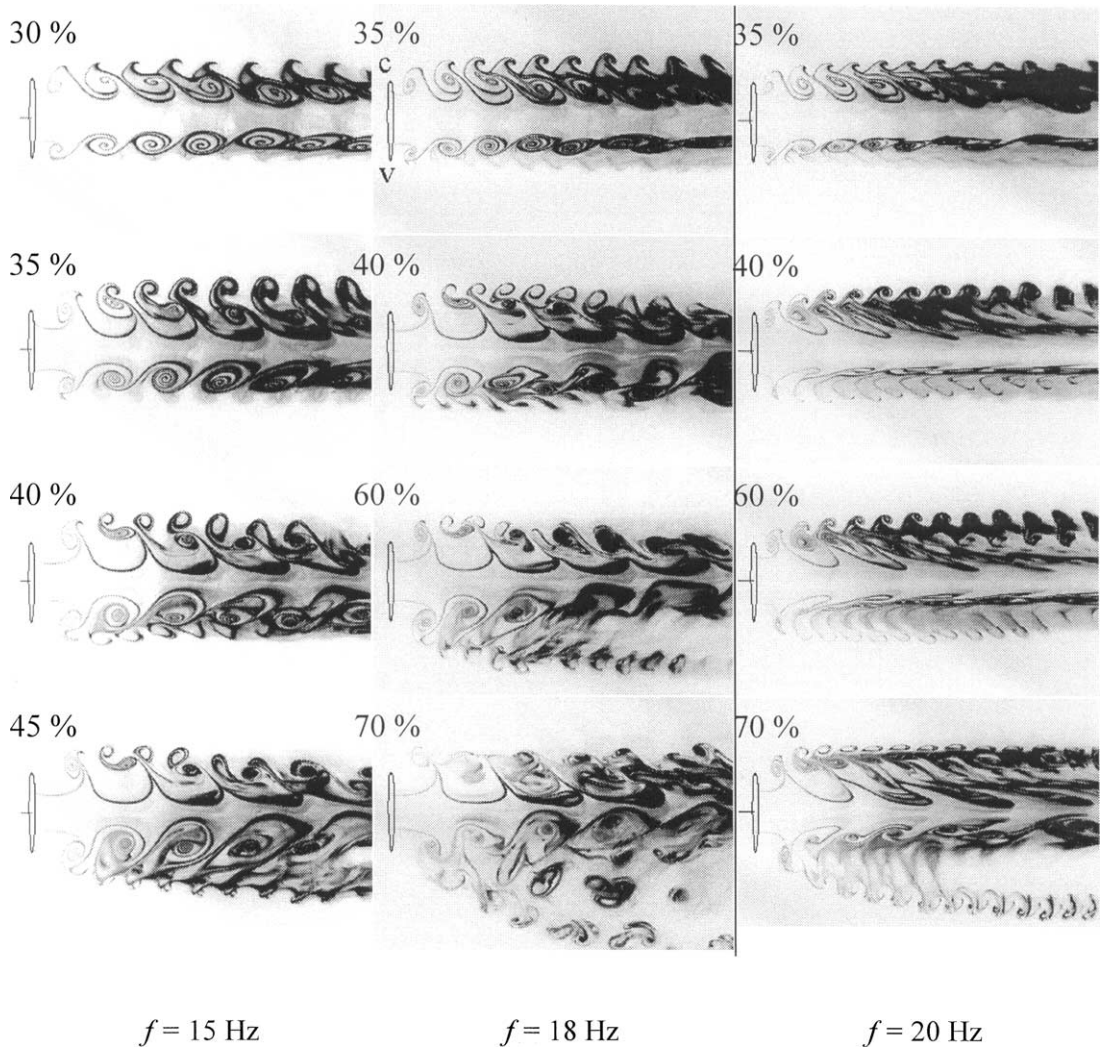

Figure 6. Longitudinal cuts along the flow axis for varying forcing amplitude. The flow conditions, as defined from equations 1, are $Re = 420$, $u_R = 0.37$. *St* are 1.1, 1.3 and 1.45 respectively. Flow comes from left to right. A crest (c) of the corrugated nozzle is on top and a valley (v) on bottom. The axial forcing amplitude for each image appears in its upper left corner.

aligned with crests and with valleys of the corrugated nozzle. The curves are well defined, because the transitions occur always in a very small range of forcing amplitudes.

Several interesting comments can be drawn from this graph. First, one can see that the appearance of a crest lateral spread does not occur for all the Strouhal number range. The threshold amplitude for that configuration remains constant or slightly decaying for medium to high Strouhal numbers, but for low numbers ($St < 1$) the configuration of crest spread disappears. In that range, the high-amplitude configuration of valley spread appears directly, while the switching process observed in *figures 5* and *6* takes place in the cases of appearance of crest spread. An additional feature is that the map shows a clear minimum of the forcing amplitude that is needed for a valley spread configuration at $St \approx 1$. Finally, if the curve of minimum forcing amplitude for the appearance of a lateral spread configuration (independent of its azimuthal location) is considered, it is fitted relatively well by a curve of the form $A_z \cdot St = C$, where C is a constant.

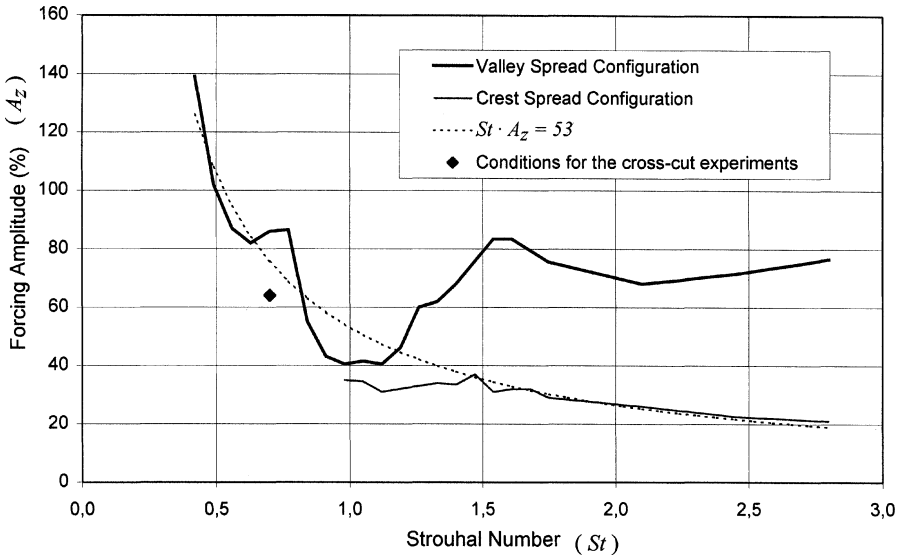

Figure 7. Map of threshold forcing amplitudes for appearance of lateral spread configurations using the corrugated nozzle.

4.2. Azimuthal organisation of the flow

The experiments in the past section focused on the organisation of the different eddies (and of the concentrations of vorticity that produce them) in a longitudinal, r–z-plane. The experiments of this section try to reveal the azimuthal organisation of the same structures.

Figure 8 shows longitudinal cuts of the flow, but only the upper part of the cut is shown. Here, the $TiCl_4$ is injected near the nozzle exit and on its outside surface, so not only the mixing layer, but also a portion of the outer jet boundary layer is shown in black. This produces a clearer visualisation of the counter-rotating eddy. The different images of *figure 8* were taken as the nozzle was rotated, so image 1 and 5 show, respectively, the flow development in azimuthal positions aligned with a crest, and with a valley of the corrugated nozzle. Images 2, 3 and 4 show intermediate azimuthal positions, moving from crest to valley. The five images give information of the azimuthal structure of the two counter-rotating vortices in different stages of their development. The conditions of the case shown here are $Re = 420$, $u_R = 0.37$, $St = 1.1$ and $A_z = 35\%$, which gives a configuration of crest spread. One can see that the primary structure is almost axisymmetric, with a slight axial delay between valley and crest aligned locations, which is probably due to the counter-rotating vortices induction. The counter-rotating vortex rings, on the other hand, develop a highly bent structure, the difference between valley and crest aligned locations increasing considerably as the flow develops. The process finishes with the lateral spread of the crest-aligned part, while the valley-aligned part is entrained by the primary vortices.

For a deeper insight on the azimuthal organisation of the two structures of azimuthal vorticity already presented, and to obtain information about the vortical structure that should develop from the secondary instability, cross cuts of the flow at different axial distances were obtained. In this case, a low forcing frequency was used to provide large wavelengths and therefore clearer images. The conditions of the experiment were $Re = 420$, $u_R = 0.37$, $St = 0.7$ and $A_z = 64\%$. Here, an indented nozzle lip was substituted for the corrugated lip. During the experiments, some evidence was gathered that the indented profile gave better results (similar flow configurations for lower forcing amplitudes). Therefore, for high amplitude experiments, it was decided to switch to the indented profile. Looking back at *figure 7*, one can see that, for the forcing conditions of the

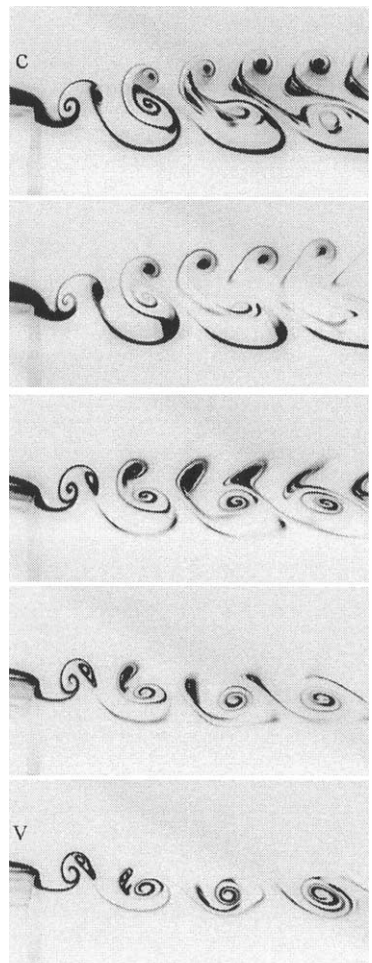

$f = 12$ Hz $A_z = 35\%$

Figure 8. Longitudinal cuts along the flow axis for varying azimuthal position from crest (top) to valley (bottom) of a corrugated nozzle. Flow from left to right.

present experiment, a corrugated nozzle cannot produce a configuration of valley spread, such as the one that appears in *figure 9*.

The longitudinal cuts of *figure 9(a)* show the axial development of the flow. The main difference with the previously observed configurations is that, for this conditions (a lower forcing frequency), the counter-rotating vortex ring cannot be observed in positions aligned with the crests. A strong wavy shape of the ring can cause this effect, which might be due to the combined effect of a more efficient azimuthal perturbation and the induction of stronger primary vortices (due to the higher forcing amplitude).

The transverse cuts of the flow at different axial positions (*figure 9(b)* to *(e)*) provide detailed information of the azimuthal structure of the flow. The primary vortex ring core develops almost axisymmetric (90(c), 180(d) and 0(e)), although around $z = 2D$ it begins to retard slightly in positions aligned with the crest of the indented profile (90(e) and even 180(e)). This last fact is also evident in the longitudinal cuts. The counter-rotating vortex ring develops a highly bent wavy shape, or so it seems by the shape of the lateral structures (180(c), 270(d)

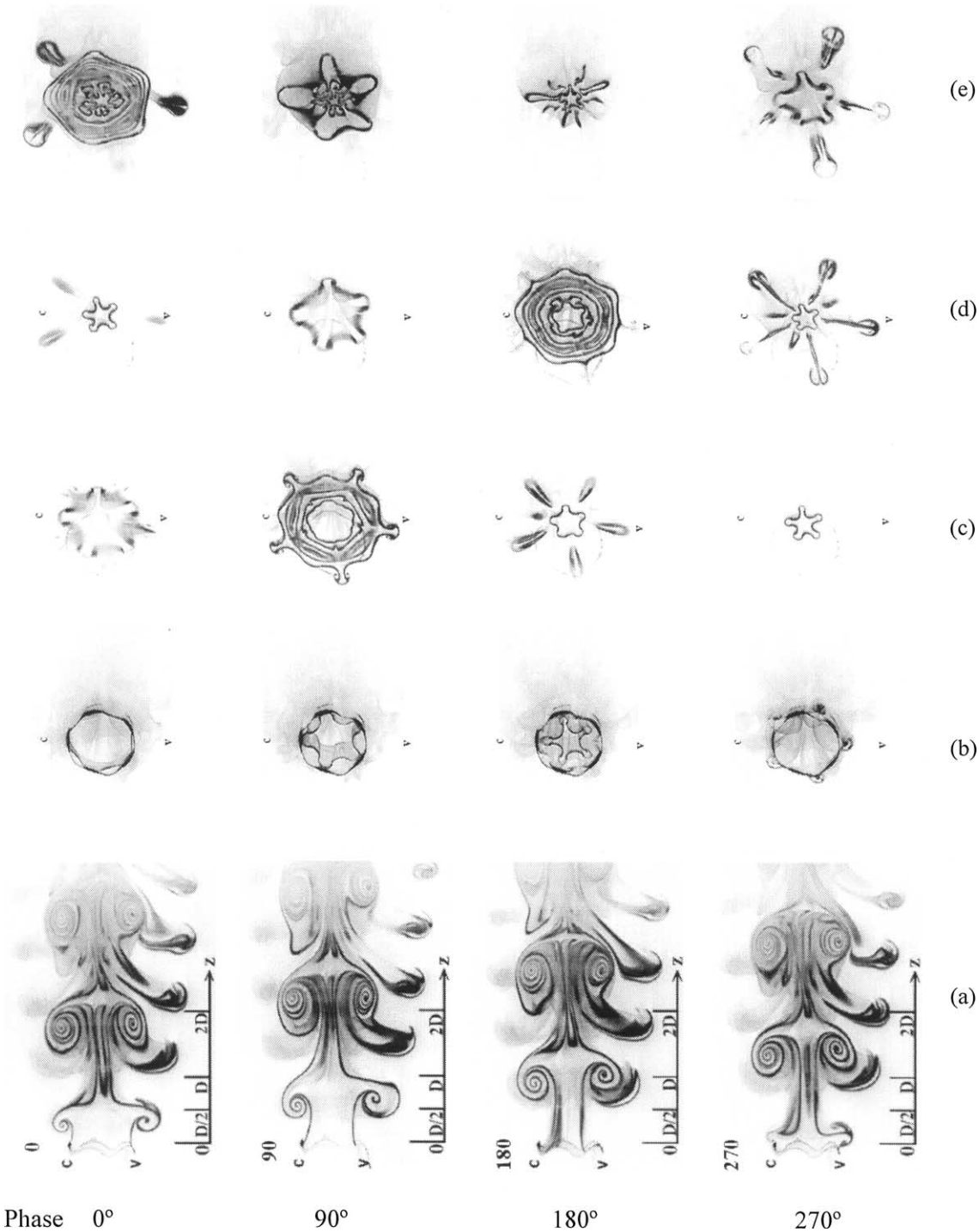

Figure 9. Longitudinal cuts along the flow axis (a) and transverse cuts at different axial distances from the indented nozzle exit: (b) $z/D = 0$, (c) $D/2$, (d) D and (e) $2D$; for 4 equi-spaced phases. In the longitudinal cuts, flow comes from bottom to top and the lobed exit can be seen in the bottom side. A crest (c) is on the left and a valley (v) on the right.

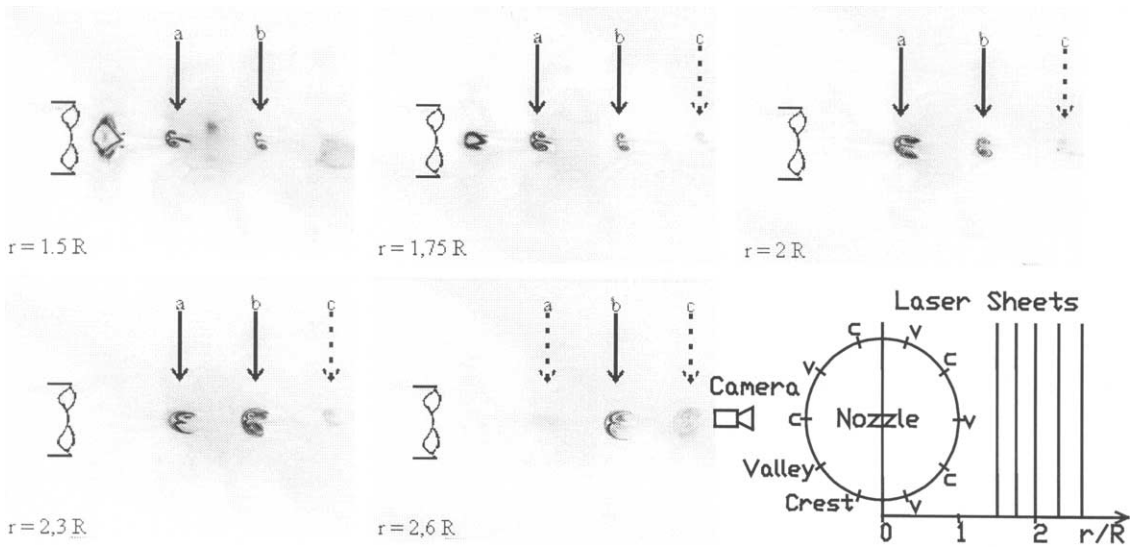

Figure 10. Longitudinal cuts on planes at different radial distances from the axial plane and parallel to it. Indented nozzle. A sketch of the layout is on the bottom right.

and 270(e)). Moreover, the secondary or streamwise structure (studied by Bernal and Roshko [15] in plane mixing layers and by Liepmann and Gharib [27] in jets) is also present. Corcos and Lin [10,11] postulated that the streamwise vortex structure would appear in all shear layers as a consequence of the stretching by the primary vortices strain field of residual vortex filaments located in the braids. The experimental evidence presented in this work support, as the afore-mentioned studies, the Corcos and Lin mechanism. Furthermore, the azimuthal perturbation imposed to the flow will permit to draw conclusions over the sign of the residual vorticity that triggers the mechanism. Lasheras and Choi [18] performed a similar study in plane shear layers. The comparison of the results is done in the next section, yielding unexpected results.

Due to the intense concentration of the primary vortices, the streamwise vortices can be even seen at the nozzle exit (90(b) and, clearer, 180(b)). 10 axial vortex filaments are present (5 pairs). In the near field, they seem to be fairly weak vortices, so the mixing layer is not rolled, but just slightly curved. Hence, the cross cuts of *figure 9* show an inner structure with the form of a rounded pentagon or a 5-point star, the vertices pointing at the crest-aligned locations. This structure appears in all cross cuts, showing that, even at an initial stage, the streamwise vortices have developed from the braids and into the primary vortices cores. Note that, in such zones, the structure may lose its form (inner part of 0(e) and 90(e) due to vortex wrap-around. A vortex reconnection process may occur in this highly stretched region, but the evidence is not precise, due to the visualization drawbacks mentioned in the introduction.

4.3. Other observations

Two interesting aspects are not well resolved in the visualisations already presented. First, the structure of the region of laterally moving fluid is difficult to unwrap. Therefore, the hypothesis of the existence of the counter-rotating ring vortex, displaying a highly bent wavy shape cannot be fully validated yet. For such purpose, *figure 10* shows longitudinal cuts of the flow on planes that are separated from the diametrical plane. With such a configuration we obtain cross cuts of the lateral structure that appears in the valleys. The visualisations show that they are formed by two adjacent counter-rotating vortices. The field of view can catch three of these structures (a), (b), (c). At $r = 2.6R$, the first structure (a) vanishes, because it has not advanced laterally enough

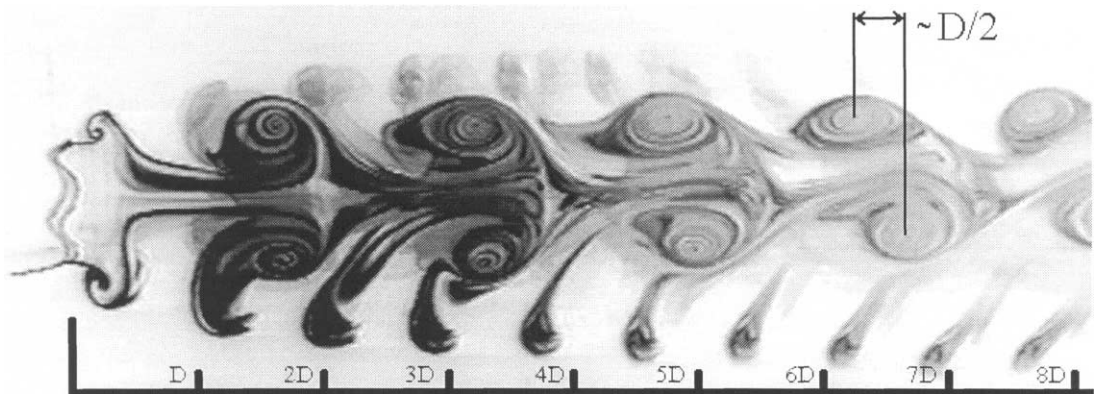

Figure 11. Longitudinal cut along the flow axis for phase 0^o. Indented nozzle. The upper structures are not crest ejection events but the out of plane shadow of adjacent valley ejection events.

yet. For larger r, all the structures in the field of view disappear. Therefore, the wavy structure of the initial counter-rotating vortex ring is now completely visualised.

On the other hand, it has been shown that, among other effects, the complex vortex dynamics tends to retard the primary vortex in crest-aligned positions. This transition to three-dimensionality of the primary (and most energetic) structure of the flow may in turn affect the transition to turbulence. *Figure 11* shows a longitudinal cut of the flow (for conditions similar to that of *figures 9* and *10*) reaching to axial positions of $8D$. The process of retardation of the crest-aligned zones of the primary vortices continuously increases, and each vortex develops a mode with wavenumber equal to 5.

5. Discussion

The results presented show the appearance and evolution in the very near field of three different types of eddies. These eddies are visualized by the deposition of an opaque substance in the mixing layer. The passive field will respond to the vorticity field that appears in the shear layer, although this inference has to be contemplated with several restraints, as summarized by Hussain [34] and others. For example, the diffusion of the passive scalar may differ strongly from that of the vorticity, and a flow can show an eddy in a place where there was vorticity, but it has long vanished. Nevertheless, the use of a periodic forcing and phase lock measurements show that the eddies observed are continuously rolling in most of the cases shown. This strengthens the assumption of the existence of a peak of vorticity at the eddy. In this section this assumption is, therefore, accepted and a reasoning is developed on this basis to try to understand the geometries observed and their evolution.

5.1. Origin of the counter-rotating vortex ring

Three different types of vortices can be found in the flow. Two of these three vortex structures have been intensively studied in the past. They are generally referred to as primary and secondary structure. Here, the axial forcing highly amplifies both vortex structures, so they concentrate in the surroundings of the nozzle exit. In this sense, the appearance of the primary vortices for large forcing amplitudes can be better understood by following the different works on vortex ring generation (the visualisations of Didden, reviewed in the album of Van Dyke ([39], plates #76 and #112), the model of vortex formation of Shariff and Leonard [40]) than as

an axisymmetric jet instability. The secondary, streamwise vortices are locked by the azimuthal perturbation and highly amplified by the primary vortex induction, which generates a strong strain field. The mechanisms involved are explained in the works of Corcos and Lin [10,11] and Lasheras and Choi [18].

The origin of the structure of counter-rotating vortex rings may be revealed in the afore-mentioned visualisations of Didden ([39], plate #76). Didden shows the formation process of a vortex ring created by a piston moving at constant speed. When the piston stops, the vortex ring detaches from the nozzle exit and then it induces a vortex ring of opposite circulation at the nozzle exit. The formation of this counter-rotating vortex is due to the radial velocities induced by the exiting vortex ring and not by suction axial velocities due to the piston (which is stopped). Therefore, an inner region of separated flow develops, shedding a free vortex. This is similar to what occurs near the trailing edge of an aerodynamic profile when the lift suddenly changes. In this case, the circulation of the vortex is connected to the change in the angle of incidence. In our case, the circulation must be connected to the locally induced velocity and the application of an unsteady Kutta condition. The application of the Kutta condition to jets has been thoroughly studied. Crighton [41] is a classical reference on this subject. Moreover, the larger circulation of the vortex ring in the valleys can be fully explained by the superposition of the ring with the hairpin vortex from the downstream secondary structure, a process that will become clear in the following graphs. In some way, this scheme follows the general concepts of the classical lifting line theory for wings, of Lanchester and Prandtl.

The similarity of our visualisations and those of Didden suggests that the main mechanism involved in the formation of the structure of counter-rotating vortex rings is this one. Nevertheless, on the present flow configuration, two other joint effects should be taken into account. First, there is an external flow, and its boundary layer provides o source of azimuthal circulation of the same sign. Ashurst and Meiburg [17] (in their simulation of the flow of Lasheras and Choi [16]) showed that it could not be neglected. The mechanism mentioned before may be affected by this extra source of vorticity, facilitating its concentration and giving way to more intense counter-rotating vortex rings.

Another mechanism is hypothesised, which is involved with the effect of the 'return' semi-period of the forcing cycle on the inner jet velocity profile. A theoretical approach to the axisymmetric velocity field of the flow in a long tube, subjected to axial forcing, was carried out to explore this effect. The aim was to study the axial velocity profile in the 'return' part of the forcing cycle. The hypothesis of a long tube (far from the exit) enables to eliminate the convection terms and the problem becomes 1D in the spatial domain. It is expected that the behaviour near the nozzle exit can be qualitatively inferred from these results. With such simplifications, the momentum equations are:

$$\frac{\partial u}{\partial t} = -\frac{1}{\rho}\frac{\partial P}{\partial x} + \nu\frac{1}{r}\frac{\partial}{\partial r}\left(r\frac{\partial u}{\partial r}\right), \qquad 0 = \frac{\partial P}{\partial r}. \tag{2}$$

The oscillating pressure gradient and the boundary conditions are:

$$-\frac{1}{\rho}\frac{\partial P}{\partial x} = A[1+\varepsilon\cos\omega t], \qquad u(R) = 0, \qquad \left.\frac{\partial u}{\partial r}\right|_{r=0} = 0,$$

where A and $A\varepsilon$ are the amplitudes of the base and forcing pressure gradients. Note that, for a useful forcing, $\varepsilon \gg 1$. This problem allows a solution of the form $u = u_0 + u_1$ where u_0 is the solution to the Poiseuille flow and u_1 is the solution to the time dependent pressure perturbation flow. The u_1 flow allows an approximate solution using perturbation theory, due to the existence of two time scales, defined by ω^{-1} and $R^2\nu^{-1}$. In our experiments, $\nu R^{-2}/\omega \sim 10^{-3}$ and therefore the viscous term can be neglected everywhere except on a very thin

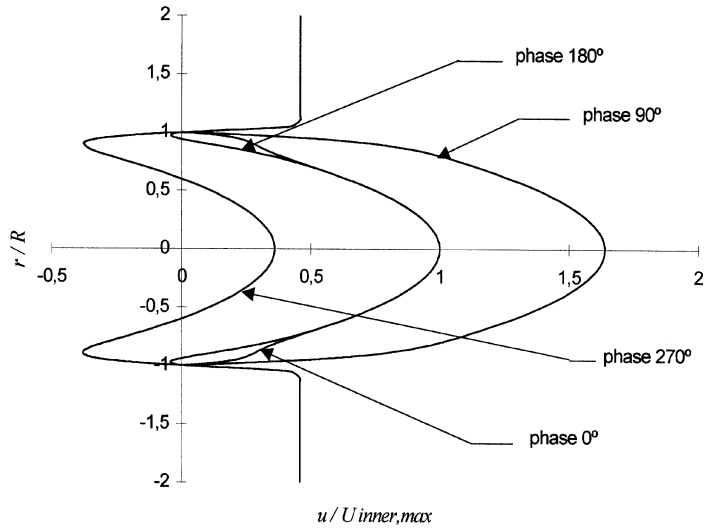

Figure 12. Profiles of non-dimensional axial velocity in the radial direction for 4 phases of the sinusoidal perturbation. $\Lambda = 1.57{\cdot}10^{-3}$, $\varepsilon = 1.02{\cdot}10^{2}$ ($St = 0.7$, $Re = 420$, $A_z = 0.64$).

layer near the duct surface. The solution has the form:

$$\frac{\Lambda\omega}{A}u(r,t) = \frac{1}{4}\left(1 - \frac{r^2}{R^2}\right) + \Lambda\varepsilon\left[\left(1 - \exp(-\Theta)\cos(\Theta)\right)\sin\omega t + \exp(-\Theta)\cos(\Theta)\cos\omega t\right], \tag{3}$$

where $\Lambda = \frac{\nu}{R^2\omega}$ and $\Theta = \frac{1-r/R}{\sqrt{2\Lambda}}$.

Figure 12 shows velocity profiles obtained from equation (2) for several phases of the sinusoidal forcing. These results suggest the existence of a complex boundary layer of the inner flow, which could enhance the circulation of the counter-rotating vortex rings by producing negative axial velocities near the inner wall.

The three different mechanisms described in this section seem to be coupled. Their relative importance has not been determined in this work. Nevertheless, the threshold curve of *figure 7* may serve to isolate the main mechanism. This curve, which represents the minimum forcing amplitude for a lateral spread configuration, is also a curve of the appearance of concentrated counter-rotating vortex rings. This is due to the experimental evidence that the lateral spread is always achieved as a result of the lateral motion of the deformed counter-rotating vortex rings. With such basis, it can be argued that the induction argument is coherent with the information of *figure 7*, and therefore it could be the main mechanism involved in the origin of the counter-rotating vortex rings. Nevertheless, the inner velocity profile behaviour explored theoretically is also compatible with this explanation, and should be coupled with the induction mechanism.

5.2. Vortex rings interactions and lateral spread of the inner jet

The primary ring has a larger circulation than the counter-rotating one. Therefore, the azimuthal perturbation will have a stronger effect on the counter-rotating vortex rings than on the primary rings, as a higher circulation precludes the advance of the azimuthal instability (Saffman [42]). Another reason for the quick-developing wavy shape of the counter-rotating rings is the presence of induction from the primary ring. It builds up a strain field, which, in turn, stretches or deforms the vortices. A scheme of this field appears in *figure 13*. Hence, the

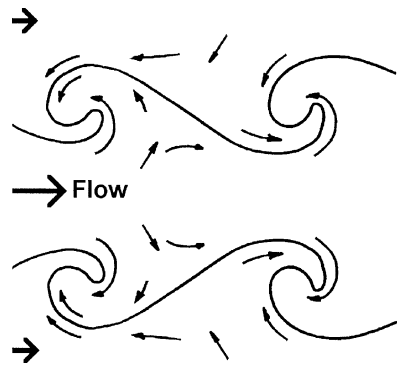

Figure 13. Scheme of the strain field produced by the array of primary vortex rings.

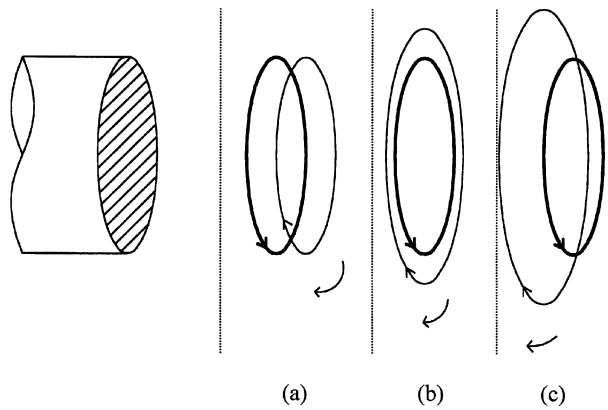

Figure 14. Expected evolution of a weak, counter-rotating, vortex ring (thin line) due to the induction of a vortex ring of larger circulation (thick line). The scheme shows the near field relative motions of the rings in the absence of azimuthal perturbation. The vertical lines remind that the configurations are a time history of the flow and not simultaneous.

counter-rotating ring will develop a highly bent wavy shape (following the mechanism proposed by Corcos and Lin [10,11]), while the primary vortex ring remains relatively axisymmetric.

To characterize the complex motion of the counter-rotating vortex ring as the flow develops downstream we will follow some preliminary steps, in order to make a clearer approach. First we consider the induced motion of a weak ring in the presence of an adjacent, more energetic ring moving over the same axis. The proposed motion is shown in the scheme of *figure 14*. The graph (a) show the initial layout of the two rings, as they appear at the nozzle exit. The weak ring appears before, induced by the previous primary ring. The subsequent primary ring appears immediately after. Then, as this new primary vortex begins its development, the weak vortex ring is induced to rotate around it (graphs (a)–(b)). On later stages (graphs (b)–(c)) two different mechanisms condition the motion of the weak ring: (i) it develops into the low velocity field of the coaxial flow; and (ii) the rotating velocities induced by the primary ring drop with the distance, as stated by the Biot-Savart law.

To clarify this mechanism, several plane schemes have been drawn and appear in *figure 15*. Here, the axial symmetry is changed to planar symmetry for clarity purposes. The scheme I-a shows a perspective view of the vortex filaments and schemes I-b-1 and 2 show crosscuts. It is shown how the velocity field created by the stronger vortex will produce a motion of the weaker vortex. Also, at the position sketched in I-b2, the weak vortex is advancing into a low velocity region, outside the mean shear layer, and another force will consequently appear.

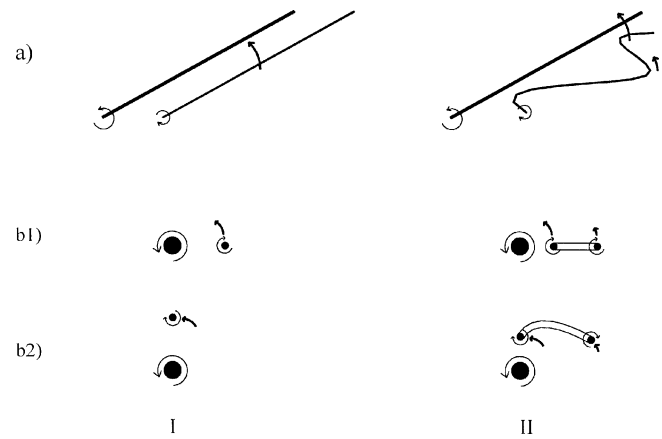

Figure 15. Schemes of the proposed evolution of a counter-rotating vortex due to the induction of a vortex of larger circulation: (I) unperturbed; (II) azimuthally perturbed; (a) perspective view; (b) spanwise view.

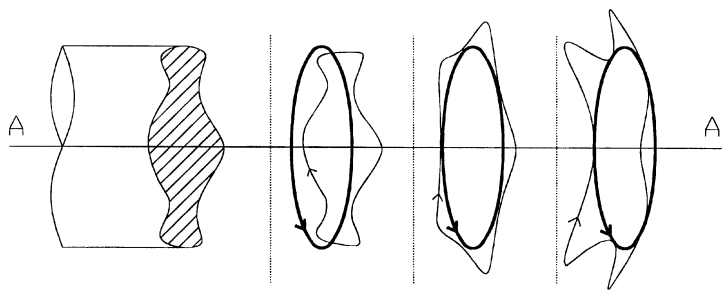

Figure 16. Proposed model of the evolution of an azimuthally perturbed counter-rotating vortex ring due to the induction of a vortex ring of larger circulation. Crest spreading configuration. Indented nozzle.

Figure 15-II shows the effect on an azimuthally perturbed vortex. The waviness of the weak vortex locates its different parts at different distances to the primary vortex. Therefore, the induced velocity will change between parts of the weak vortex, producing its stretching. This mechanism is best shown in II-b. This effect, added to the expected global motion shown in *figure 14*, will produce the different local expansion of the mixing layer in each azimuthal location.

Figure 16 shows a similar scheme that the one in *figure 14*, but the effect of the azimuthal perturbation on the weak ring is considered here. The axial combing of the weak ring observed in the sketch of *figure 15* II-b2 is not shown in order to get a simpler scheme, but its implications on the passive scalar field will be shown in the following figures. *Figure 16* shows the limit case in which some zones of the counter-rotating ring are swallowed in the primary ring core. This configuration can be observed in the images of *figure 9*. The images of *figures 5* and *6* show intermediate configurations to those depicted in *figures 14* and *16*.

Although the scheme of *figure 16* is quite simple, its implications on the passive scalar field (the mixing layer), as visualised, are not so straightforward. Therefore, a sketch is presented in *figure 17*, and it shows good agreement with the experimental data of *figure 9*.

The question of the azimuthal organisation of the zones of lateral spread must now be addressed. *Figures 16* and *17* showed a crest spread case, which occurs for low forcing amplitudes. The analysis of extensive visualisations for high forcing amplitude cases allows explaining the mechanism that takes place when the spread location is displaced to the valleys. *Figure 18* shows three sketches for the three different cases: crest

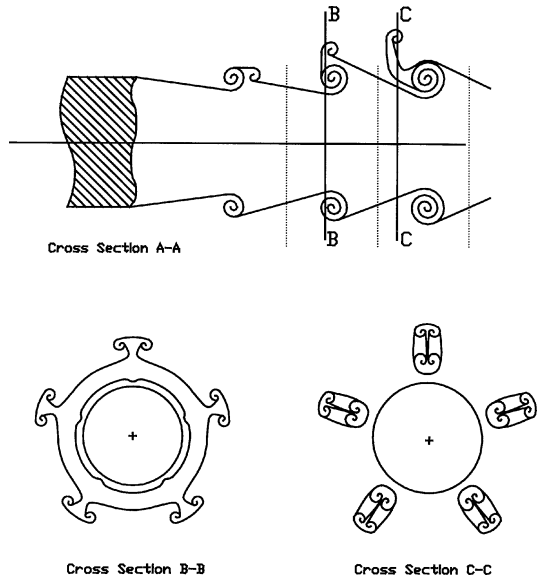

Figure 17. Representation of the forced mixing layer structure for the configuration shown in *figure 16*. The longitudinal cut represents section AA in the named figure and the position of the transverse sections BB and CC occur in the positions defined in the longitudinal cut. Vertical lines in section AA are put to recall that the axial positioning is not the actual relative position, and it only represent a time history of the structure.

spread (a), valley spread (b) and both valley and crest spread (c). This last case was experimentally observed for the first time by Lasheras et al. [32] and called 'doubling mode'. A full description of the different modes can now be achieved. The switching mechanism shows a direct dependence on the velocity field near the nozzle exit lip at the time of the concentration of the counter-rotating vortex ring. The cases (a) and (b) of *figure 18* are limit situations and (c) is an intermediate case. The argument is that, for low amplitude forcing, the weak ring concentrates and moves axially downstream (the cylindrical symmetry has been turned to plane symmetry in the graph for a clearer understanding); while, for a high amplitude forcing, its motion has a considerable radial component. The previous primary vortex ring, which induces the radial velocity in the nozzle lip, has a circulation that is amplitude dependent. Increasing the forcing amplitude will produce vortex rings (both) of larger circulation, as the overall circulation of the shear layer is a constant and it is equal (in a forcing wavelength) to the subtraction of the circulations of the two rings. Therefore, by increasing the forcing amplitude the configurations obtained at the nozzle exit will change gradually from graph (a) to (c) and then to (b). After the weak ring has drifted away (in the prescribed direction for each case), the new primary vortex ring begins to concentrate in the nozzle exit lip. Due to its induction, the weak ring will move as shown in the second part of the three graphs. Note that, depending on the initial drift of the counter-rotating ring, different zones of it become the nearest to the primary ring, and hence the spread location differs in each case as expected. Case (c) is slightly more complex, as the counter-rotating ring is forced to rotate around an intermediate zone between valley and crest, which causes the doubling of the spread locations.

Finally, each of the processes can produce the ejection of a closed vortex loop, as proposed by Martin and Meiburg [28] and Lasheras et al. [32]. A sketch of the mechanism proposed as an explanation is shown in *figure 19*. The weak, counter-rotating ring is partially swallowed by the strong ring, except in the surroundings of the lateral spread location. The induction of both vortices may produce a stretching of the weak filament (graph b) and it might lead to its annihilation and the reconnection in two vortices (graph c). Then, the closed vortex loop will drift away, self-propelled, and the remains of the former counter-rotating ring will slowly fade away and be swallowed by the primary ring. This mechanism differ with those proposed in [28] and [32] in

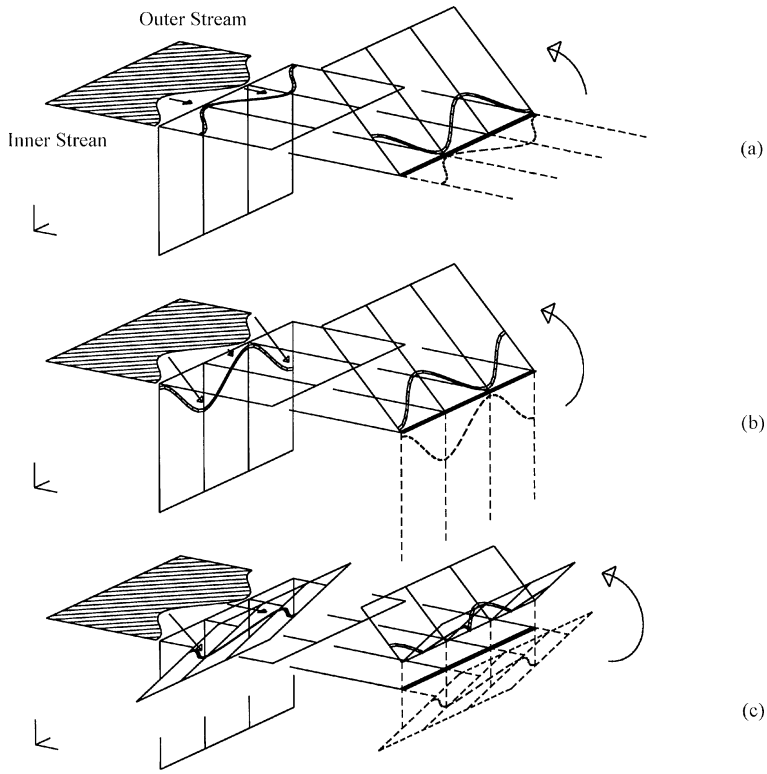

Figure 18. Scheme of the processes that lead to the different azimuthal locations of the laterally spreading zones. The cylindrical configuration has been substituted for plane configuration for clarity purposes, but the inference of the actual geometry is straightforward.

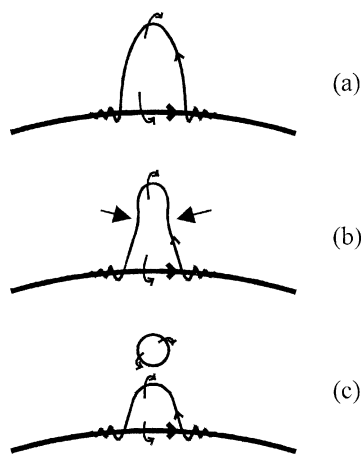

Figure 19. Mechanism of an ejection event through reconnection of adjacent sides of the stretched weak (counter-rotating) vortex ring.

that the reconnection will take place between filaments of the highly stretched counter-rotating ring, instead of the primary ring. These features can eventually be observed in some of the high amplitude images of *figures 5* and *6*. Nevertheless, a vortex reconnection cannot be inferred from the visualization of a scalar. The process may take place, but there is no experimental evidence at this time.

5.3. Evolution of the secondary, or streamwise, structure

The nature and evolution of the secondary structure, as can be seen in the images, resembles to that in the unforced case (as shown by Liepmann and Gharib [27] and others). But the apparition of counter-rotating vortex rings is linked with strong forcing conditions. Therefore, the secondary structure can only remain unchanged if it does not interact strongly with the counter-rotating vortex rings. This independent development seems reasonable owing to their relative locations: the counter-rotating vortex ring appears in the vicinity of the primary vortex ring and moves radially outwards, while the secondary structure appears in the braids and expands towards the cores of the two adjacent primary vortex rings.

The study of the unforced flow by Liepmann and Gharib [27] presented a general similitude with the secondary structure observed in plane shear layers by Bernal and Roshko [15] and others. Their visualisations (and velocity measurements) support the mechanism postulated by Lin and Corcos [11] for the development of a secondary instability in free shear flows. Furthermore, Lasheras and Choi [18] explored a transversally perturbed plane layer to show that the origin of the secondary structure could be found in a residual, spanwise, braid vortex. In our case, the azimuthal perturbation imposed at the nozzle lip enables to follow a similar reasoning, which is sketched in *figure 20*. In our quasi-axisymmetric flow, the organisation of the streamwise structure forms a rounded five-point star with the vertices aligned with the crests of the nozzle exit (c). This fact, associated with the requirement that a continuous, but strongly waved, vortex filament must form the secondary structure (Lin and Corcos [11]), defines the sign of the original vortex filament. It must be a vortex ring and its circulation must be opposite to that of the primary ring. This result is surprising and encouraging, because it postulates the existence of different mechanisms for the origin of the secondary structure in co-flowing jets than for the plane shear layer. The preponderance of such a sign of circulation in the braids has to been checked thoroughly and is fully compatible with the images here present and with numerical results as those presented by Martin and Meiburg [28]. Detailed experiments for low forcing and unforced conditions are currently taken place and will be the basis of a future article.

With the inclusion of the secondary structure, the qualitative modelling of the flow is now complete. *Figure 21(a)* shows a revision of *figure 16*, with the addition of the secondary structure. *Figure 21(b)* shows the related arrangement over the primary vortex ring of the filaments that conform the counter-rotating vortex ring and the secondary structure. *Figure 22* shows the effect of such vortex arrangement in the mixing layer. These

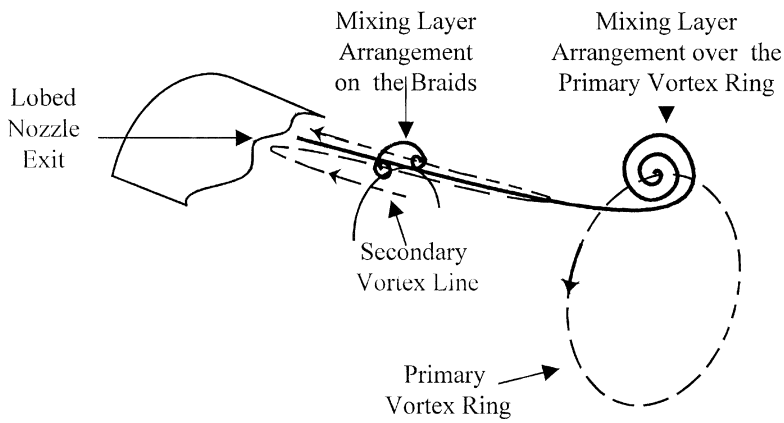

Figure 20. Sketch of the braid arrangement of the secondary structure, showing that the initial residual vortex ring that develops in the strain field to form the structure should be counter-rotating.

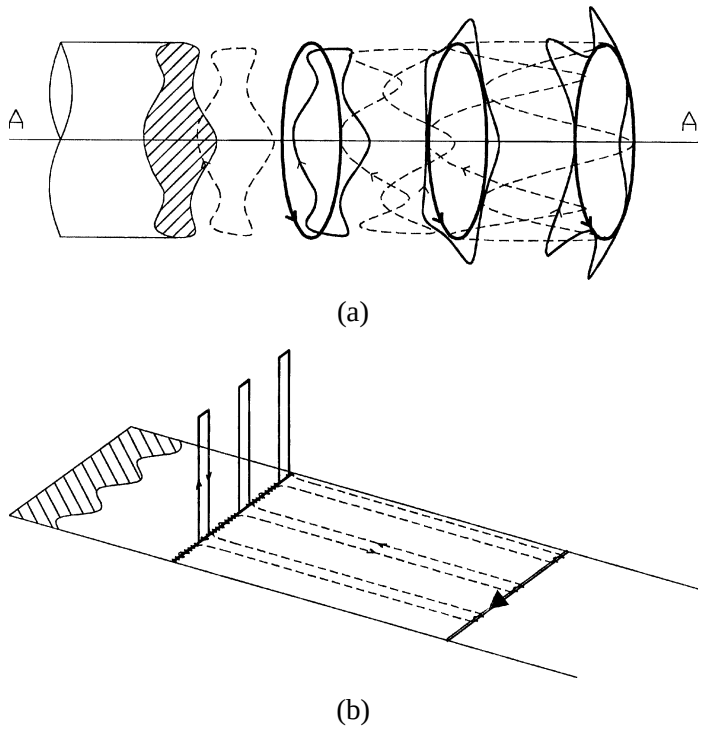

Figure 21. Proposed model of the two weak structures evolution, showing the amplification of their initial wavy shape in the primary vortices strain field. The primary structures are represented by a thick line, the weak vortex rings by a thin line and the secondary structure by a dotted line. The flow configuration corresponds to a crest-spread case: (a) three-dimensional sketch; (b) plane simplification to show the possible interaction between the three structures.

two figures show a flow configuration that leads to a crest spread. The longitudinal sketch of *figure 22* shows a good agreement with the low forcing amplitude images of *figures 5* and *6*.

Similar sketches have been obtained for valley spread configurations, such as those shown in the high forcing amplitude images of *figures 5* and *6* and in the images of *figure 9*. They appear in *figures 23* and *24*. Note that *figure 23(b)* shows a complex interaction between the two weak vortex structures at the surroundings of the upstream primary vortex ring. This interaction did not appear in the crest spread case because the azimuthal arrangements of the two structures was interleaved in the zone, a situation that is modified as the counter-rotating vortex ring switches its azimuthal position.

The sketches of *figure 24* can be compared to the images obtained for the experimental conditions of *figure 9*, yielding a full agreement. Therefore, the proposed three-structure model of the flow can be considered adequate.

5.4. Primary vortex ring transition to three-dimensionality

The transition to three-dimensionality of the primary vortex ring (*figure 12*) can be explained as a consequence of the development of the secondary structure into the cores of two adjacent primary vortex rings. Lasheras and Choi [18] described a similar process in plane shear layers. Two sketches have been drawn, for the two cases of valley and crest spread. They appear in *figure 25*. Note that the wavy shape of the primary ring is independent on the lateral spread configuration, as it only depends on the secondary structure organisation, which remains invariant.

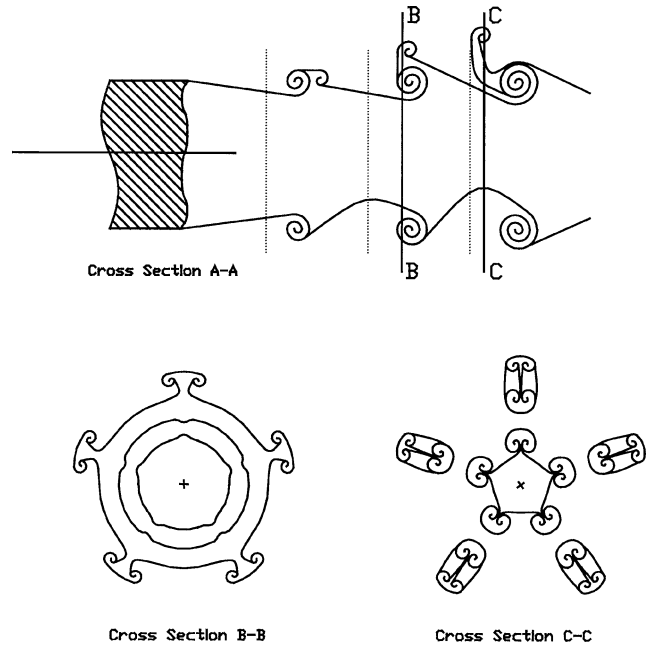

Figure 22. Representation of the forced mixing layer structure for the configuration shown in *figure 21* (crest-spread case). The longitudinal cut represents section AA in the named figure and the position of the transverse sections BB and CC occur in the positions defined in the longitudinal cut.

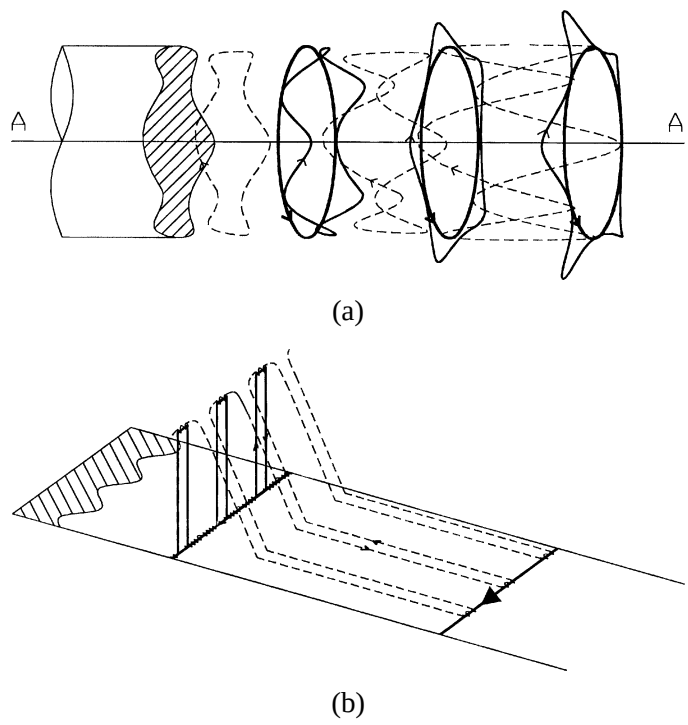

Figure 23. Proposed model of the two weak structures evolution, showing the amplification of their initial wavy shape in the primary vortices strain field. The primary structures are represented by a thick line, the weak vortex rings by a thin line and the secondary structure by a dotted line. The flow configuration corresponds to a valley-spread case: (a) three-dimensional sketch; (b) plane simplification to show the possible interaction between the three structures.

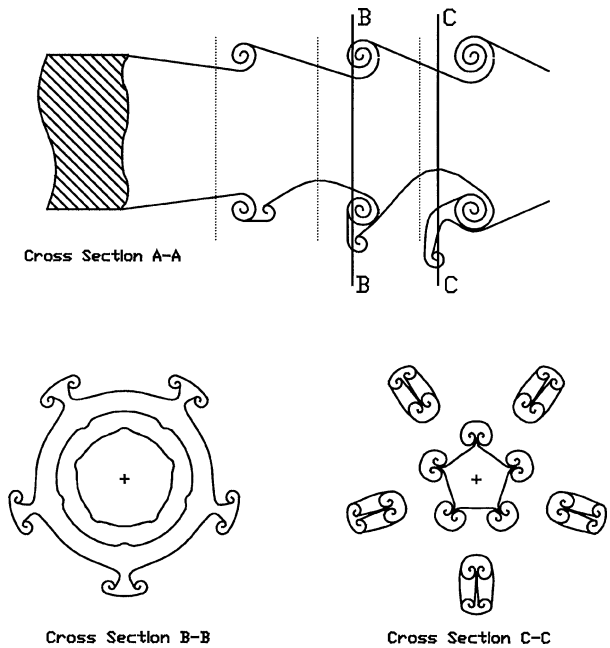

Figure 24. Representation of the forced mixing layer structure for the configuration shown in *figure 23* (valley-spread case). The longitudinal cut represents section AA in the named figure and the position of the transverse sections BB and CC occur in the positions defined in the longitudinal cut.

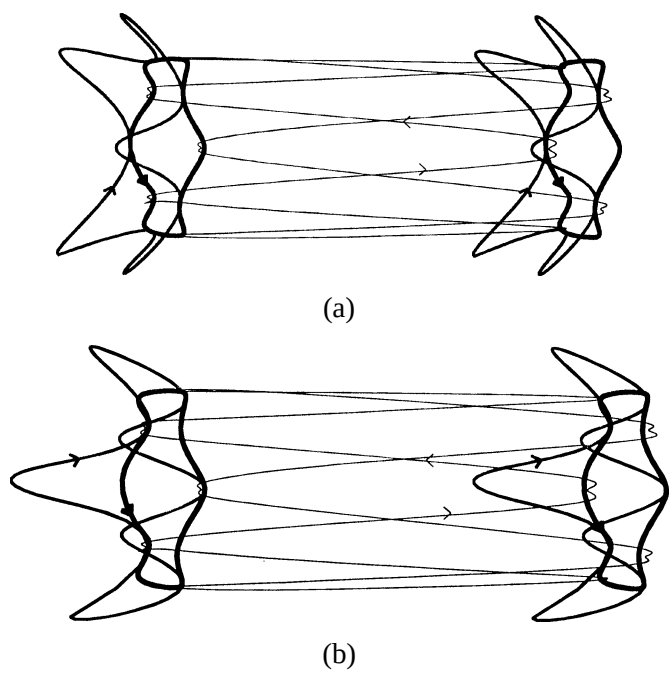

Figure 25. Secondary structure organisation between adjacent primary vortices and its final effect on its three-dimensional transition. Note that the configurations are similar in (a) the valley-spread case, and (b) the crest-spread case.

6. Conclusions

The effect of a monochromatic, finite amplitude inner forcing in the development of co-flowing jets is analysed. The flow development is observed to change considerably as compared to the unforced case, and lateral spread configurations occur.

Three different flow structures have been distinguished and, due to the strong axial forcing, they all appear in the surroundings of the nozzle exit as concentrated vortices. Two of the structures are the well-known primary and secondary structures that appear in the natural jet, although amplified by the forcing. The third structure is only present for high forcing conditions. It appears on the nozzle exit as another array of vortex rings, interleaved with the primary structure's array. The circulation of these new vortices is smaller and of opposite sign as compared with the primary vortex ring. Therefore, they are named counter-rotating vortex rings throughout the article. Three mechanisms have been suggested as involved in the formation of the counter rotating vortex ring structure. Probably, the different mechanisms are coupled. Nevertheless, the strong dependence of the structure on the forcing parameters suggests that the main mechanism is the induction of radial velocities near the nozzle exit by a previous primary vortex.

The development of the three structures involves strong interactions between both the two weak structures and the primary and more energetic structure, which induction field dominates the flow. The different processes have been qualitatively modelled. They seem to mainly respond to inviscid processes following the laws of Helmholtz and Biot-Savart. The most interesting result is that, for certain condition, the flow is observed to expand laterally (radially) in an almost explosive way.

An azimuthal perturbation was imposed on the nozzle lip and the azimuthal arrangement of the weak flow structures was studied, enabling a clearer understanding of their dynamics. The secondary structure shows an invariant organisation, independent of the forcing parameters, while the azimuthal arrangement of the counter-rotating vortex rings depends on them. The velocity field existing in the nozzle exit at the moment of concentration of the vortex seems to be of paramount importance in the azimuthal locking of the structure of counter-rotating vortex rings. A balance between the radial and axial (convective) velocities in the zone, gives three possible cases. The azimuthal organisation of the counter-rotating ring can thus be symmetric or anti-symmetric to that of the secondary structure (which remains invariant). The third case is a combination of these two. The different azimuthal organisation of the counter-rotating ring gives way to three lateral spreading configurations that differ from each other in the location and number of spreading zones. The different cases depend strongly on the forcing amplitude. The Strouhal number is also important, as it defines the wavelength of the primary structure. A map of the different configurations depending on these two parameters was obtained from extensive visualisations.

A qualitative model of the three-dimensional vortex dynamics has been proposed using inviscid dynamic arguments. The model can explain the different configurations of the flow field, giving a complete agreement with experimental evidence.

References

[1] Michalke A., Freymuth P., The instability and the formation of vortices in a free shear layer, AGARD Conf. Proc. 4 (2) (1966)
[2] Becker H., Massaro T., Vortex evolution in a round jet, J. Fluid Mech. 31 (1968) 435–448.
[3] Beavers G.S., Wilson T.A., Vortex growth in jets, J. Fluid Mech. 44 (1970) 97–112.
[4] Crow S., Champagne F.M., Orderly structure in jet turbulence, J. Fluid Mech. 48 (1971) 547–591.
[5] Cohen J., Wygnanski I., The evolution of instabilities in the axisymmetric jet. Part 1. The linear growth of disturbances near the nozzle, J. Fluid Mech. 176 (1987) 191–202.
[6] Yule A.J., Large scale structure in the mixing layer of a round jet, J. Fluid Mech. 89 (1978) 413–432.

[7] Tso J., Hussain F., Organized motions in a fully developed turbulent axisymmetric jet, J. Fluid Mech. 203 (1989) 425–448.
[8] Widnall S.D., Bliss D.B., Tsai C.Y., The instability of short waves on a vortex ring, J. Fluid Mech. 66 (1974) 35–47.
[9] Maxworthy T., Some experimental studies of vortex rings, J. Fluid Mech. 81 (1977) 465–495.
[10] Corcos G.M., Lin S.J., The mixing layer: Deterministic models of a turbulent flow. II – The origin of the three-dimensional motion, J. Fluid Mech. 139 (1984) 67–95.
[11] Lin S.J., Corcos G.M., The mixing layer: Deterministic models of a turbulent flow. III – The effect of plane strain on the dynamics of streamwise vortices, J. Fluid Mech. 141 (1984) 139–178.
[12] Alvarez C., Martinez-Val R., Visual measurements of streamwise vorticity in the mixing layer, Phys. Fluids 27 (1984) 2367.
[13] Neu J.C., The dynamics of stretched vortices, J. Fluid Mech. 143 (1984) 253–276.
[14] Jimenez J., Cogollos M., Bernal L.P., A perspective view of the plane mixing layer, J. Fluid Mech. 152 (1985) 125–143.
[15] Bernal L.P., Roshko A., Streamwise vortex structure in plane mixing layers, J. Fluid Mech. 170 (1986) 499–525.
[16] Lasheras J.C., Cho J.S., Maxworthy T., On the origin and evolution of streamwise vortical structures in a plane, free shear layer, J. Fluid Mech. 172 (1986) 231–258.
[17] Ashurst W.T., Meiburg E., Three-dimensional shear layers via vortex dynamics, J. Fluid Mech. 189 (1988) 87–116.
[18] Lasheras J.C., Choi H., Three-dimensional instability of a plane shear layer: an experimental study of the formation and evolution of streamwise vortices, J. Fluid Mech. 189 (1988) 53–86.
[19] Huang L., Ho C., Small-scale transition in a plane mixing layer, J. Fluid Mech. 210 (1990) 475–500.
[20] Nygaard K.J., Glezer A., Evolution of streamwise vortices and generation of small-scale motion in a plane mixing layer, J. Fluid Mech. 231 (1991) 257–301.
[21] Bell J.H., Mehta R.D., Measurements of the streamwise vortical structures in a plane mixing layer, J. Fluid Mech. 239 (1992) 213–248.
[22] Lasheras J.C., Meiburg E., Experimental and numerical investigation of the three dimensional transition in plane wakes, J. Fluid Mech. 190 (1988) 1–30.
[23] Bays–Muchmore B., Ahmed A., On streamwise vortices in turbulent wakes of cylinders, Phys. Fluids A 5 (2) (1993) 387–392.
[24] Mansy H., Yang P., Williams D.R., Quantitative measurements of three-dimensional structures in the wake of a circular cylinder, J. Fluid Mech. 280 (1994) 277–296.
[25] Williamson C.H.K., Three-dimensional wake transition, J. Fluid Mech. 328 (1996) 345–407.
[26] Agui J.C., Hesselink L., Flow visualization and numerical analysis of a co-flowing jet – A three-dimensional approach, J. Fluid Mech. 191 (1988) 19–45.
[27] Liepmann D., Gharib M., The role of streamwise vorticity in the near field entrainment of a round jet, J. Fluid Mech. 245 (1992) 643–668.
[28] Martin J.E., Meiburg E., Numerical investigation of three-dimensionally evolving jets subject to axisymmetric and azimuthal perturbations, J. Fluid Mech. 230 (1991) 271–318.
[29] Grinstein F., Gutmark E., Parr T., Hanson-Parr D., Obeysekare U., Streamwise and spanwise vortex interaction in an axisymmetric jet, Phys. Fluids 8 (1996) 1515–1524.
[30] Brancher P., Chomaz J.M., Huerre P., Direct numerical simulations of round jets: Vortex induction and side jets, Phys. Fluids 6 (5) (1994) 1768–1774.
[31] Williamson C.H.K., Vortex dynamics in the cylinder wake, Annu. Rev. Fluid Mech. 28 (1996) 477–539.
[32] Lasheras J.C., Liñan A., Lecuona A., Rodríguez P., Vorticity dynamics in three-dimensional pulsating co-flowing jet diffusion flames, in: Jiménez J. (Ed.), 24th Symposium on Combustion. The Global Geometry of Turbulence, NATO ASI Series B, Vol. 268, 1992, pp. 325–332.
[33] Monkewitz P.A., Pfizenmaier E., Mixing by 'side jets' in strongly forced and self-excited round jets, Phys. Fluids A 3 (1991) 1356–1360.
[34] Hussain A.K.M.F., Coherent structures and turbulence, J. Fluid Mech. 173 (1986) 303–356.
[35] Ruiz-Rivas U., Lecuona A., Rodriguez P.A., Nogueira J.I., PIV Measurements in co-flowing jets subjected to axial forcing: Vorticity and strain field structure, Selected Papers of the 10th International Symposium on Applications of Laser Techniques to Fluid Mechanics, Lisbon 2000, Springer-Verlag (to be published).
[36] Prestidge K., Vorticity Dynamics and Lateral Ejections in Strongly Forced Lobed Jets. PhD thesis, University of San Diego.
[37] Prestidge K., Lasheras JC., Three dimensional vorticity dynamics in a coflowing, turbulent jet subjected to axial and azimuthal perturbations, in: Euro. Series in Applied and Industrial Mathematics, Vol. 1, 1996, pp. 553–564.
[38] Pierrehumbert R.T., Widnall S.E., The two- and three-dimensional instabilities of a spatially periodic shear layer, J. Fluid Mech. 114 (1982) 198–210.
[39] Van Dyke M., An Album of Fluid Motion, Parabolic Press, Stanford, 1982.
[40] Shariff K., Leonard A., Vortex rings, Annu. Rev. Fluid Mech. 24 (1992) 235–279.
[41] Crighton D.G., The Kutta condition in unsteady flow, Annu. Rev. Fluid Mech. 17 (1985) 411–445.
[42] Saffman P., Vortex Dynamics, Cambridge University Press, Cambridge, 1992.